Nonlinear model predictive control with logic constraints for COVID-19 management

Tamás Péni · Balázs Csutak · Gábor Szederkényi · Gergely Röst

Abstract The management of COVID-19 appears to be a long term challenge, even in countries that have managed to suppress the epidemic after their initial outbreak. In this paper, we propose a model predictive approach for the constrained control of a nonlinear compartmental model that captures the key dynamical properties of COVID-19. The control design uses the discrete-time version of the epidemic model, and it is able to handle complex, possibly time-dependent constraints, logical relations between model variables, and multiple predefined discrete levels of interventions. A state observer is also constructed for the computation of non-measured variables from the number of hospitalized patients. Five control scenarios with different cost functions and constraints are studied through numerical simulations, including an output feedback configuration with uncertain parameters. It is visible from the results that, depending on the cost function associated to different policy aims, the obtained controls correspond to mitigation and suppression strategies, and

T. Péni
Institute for Computer Science and Control (SZTAKI), H-1111 Budapest, Kende u. 13-17.
E-mail: peni.tamas@sztaki.hu
and
Department of Control for Transportation and Vehicle Systems, Faculty of Transportation
Engineering and Vehicle Engineering, Budapest University of Technology and Economics,
H-1111 Stoczek u. 2., Budapest, Hungary

G. Szederkényi and B. Csutak
Faculty of Information Technology and Bionics, Pázmány Péter Catholic University
H-1083 Práter u. 50/a, Budapest, Hungary
E-mail: {csutak.balazs, szederkenyi}@itk.ppke.hu
and
Institute for Computer Science and Control (SZTAKI), H-1111 Budapest, Kende u. 13-17.

G. Röst (✉)
Bolyai Institute, University of Szeged, H-6720 Szeged, Hungary
E-mail: rost@math.u-szeged.hu

the constructed control inputs are similar to real life government responses. The results also clearly show the key importance of early intervention, the continuous tracking of the susceptible population and that of future work in determining the true costs of restrictive control measures and their quantitative effects.

Keywords COVID-19 · epidemic model · disease control · differential equations · control theory · model predictive control · temporal logic

1 Introduction

On December 31, 2019, China alerted the World Health Organization (WHO) on a cluster of pneumonia cases of unknown origin in Wuhan, China. On January 7, 2020, the causative pathogen of the outbreak was identified as a novel coronavirus, later named as SARS-CoV-2, and the disease it causes as COVID-19. SARS-CoV-2 infections quickly spread : the first case outside China was identified in Thailand, on 14 January, followed by reported cases from a number of countries [6,55].

In Europe, the first cases were confirmed on January 24, 2020 in France (where, later in April, COVID-19 was retrospectively confirmed for a patient hospitalized in late December 2019) [49,13], and on January 27, in Germany, Bavaria, leading to a local outbreak [7]. The first epidemic in Europe started in the Lombardy region of Italy with the first detection on February 20, 2020 [45]. Control measures started in mid-March in most of the European countries, including social distancing measures that reflect strong effort to suppress, or at least to slow down the spreading of COVID-19. Because of the differences in timing and stringency of the applied measures, the peak daily incidence varied substantially among countries, and recently a resurgence of cases have been observed [17]. By the end of July 2020, around seventeen million cases and seven hundred thousand deaths have been reported worldwide, with significant spreading in the Americas, Eastern Mediterranean and Southeast Asia [56].

In the absence of vaccine and effective treatment, the non-pharmaceutical intervention strategies can roughly be divided into two main categories. Mitigation does not aim to completely stop the transmission of the virus, only to slow down to keep the number of infected people below the capacity of the healthcare system. Sweden is an example of such strategy. On the other hand, suppression aims to reduce the incidence to a very low level by strict social distancing, and then keep that number low by localized and targeted measures, such as efficient surveillance, testing, tracing and quick isolation of cases. The first outbreak was suppressed in most European and East Asian countries, Australia, and New Zealand. Recently, following a relaxation of such measures, a resurgence has been observed in the Western Balkans [17].

Mathematical models have been commonly used in epidemiology to evaluate disease control strategies. However, disease control in this context usually refers to a single intervention measure that is sufficient to reduce the reproduction number below one, leading to the eradication of the disease. The most

commonly used measures are vaccination and drug treatment [19], or, in the case of vector borne diseases, culling of mosquitoes and other arthropods that transmit the pathogen into other living organisms. The current COVID-19 situation is unprecedented in the sense that governments are constantly tuning their control measures, trying to find balance between public health concerns and the costs of social distancing measures to the society and the economy. Thus, using feedback, which is a standard tool in control theory, is necessary to dynamically manage our response to the pandemic, and tailor policies to stabilize the situation.

In a control theory framework, dynamical systems are considered as operators mapping from an input signal (function) space to an output space [47]. We distinguish between manipulable inputs which can be set (often between certain limits) by the user and disturbance inputs from the environment that cannot be directly influenced. The outputs are either directly measured quantities or they are computed from measurements. The control goals are usually prescribed using the outputs, e.g. they have to track a reference trajectory or just stay between predefined limits. Such goals are often equipped with additional constraints and optimality criteria. Possible examples for the former are (physical) bounds on the inputs and/or on the state variables, and minimal control cost or operation time for the latter. Therefore, a complex control problem can be most often expressed in the form of constrained optimization.

Even the simplest epidemic models are nonlinear which makes the corresponding control problems challenging due to complex dynamical behaviour, possible singularities and the state dependent nature of fundamental properties like reachability or observability [29]. Parameter and input uncertainties, or the lack of measurements of sufficient quality often add further difficulties to the problem [43,41].

There is a wide literature on the model-based targeted manipulation of diseases either within the host or across an entire population [4,26,1,40,52]. In [8], model predictive control is used for the optimal allocation of vaccination resources between different risk groups and regions. A robust model predictive approach for stochastic epidemic models is proposed in [53], where quarantine policy design is shown as a possible control input. Detailed control related model analysis and vaccination input design is proposed in [12] which tracks a prescribed output given in terms of susceptible and infected people. A quantitative model is presented in [51] for the COVID-19 outbreak in Wuhan, China, taking into consideration the effect of different interventions. In [22] an 8-compartment ODE model is presented for describing and analyzing the COVID-19 epidemic in Italy, where the authors show different scenarios for the implementation of countermeasures. The same model structure is used in [31] adapted to the data from Germany. A model predictive control approach is proposed, and it is shown that the number of fatalities can be significantly reduced even when the model and some measurements are uncertain. Vast majority of the available control approaches assume a control input with continuous range which is clearly useful for strategic planning, but not straightforward to put into practice if there are distinct levels of inter-

vention. A notable exception is [36], where starting and stopping strict social distancing is a binary control input applied in a nonlinear model predictive framework, and tested through simulations on nominal and uncertain models of the COVID-19 pandemic in Brazil.

Most advanced feedback control methods need the whole state information for computing the input, but it is not realistic to assume that the number of individuals in each compartment can be continuously measured (especially latent, asymptomatic or even mildly symptomatic people). Therefore, a state estimator is needed in practice, which is known to be non-trivial to design for nonlinear systems, and most often its stability has to be proved on a case by case basis [29]. A general observer class with convergence proof is proposed for low-dimensional continuous time epidemic models in [28]. An implicit observer design approach for specially discretized SEIR models with global convergence proof is described in [27].

Temporal logic provides a powerful framework for the modeling, analysis and control of discrete time dynamical systems, which is a correct-by-construction approach [5]. Using signal temporal logic, complex specifications and constraints can be given for the required dynamical behaviour of a model in a compressed form. A particularly successful application of this computation framework is model predictive control, where the requirements can be automatically translated to a mixed integer programming problem taking into consideration the system dynamics as constraints [18]. Most often, linear dynamical models are preferred for control design with temporal logic, since those can be put into the framework of mixed integer linear programming. However, there exist really powerful solvers capable of efficiently handle nonlinear models as well [32].

Based on the above, the aim of this paper is to propose an optimization-based control approach for compartmental epidemic models constructed for the COVID-19 outbreak, which is able to take into account complex, possibly time-dependent specifications including bounds, and even logical relations between model variables, and multiple predefined discrete levels of interventions. Another important goal is to study the possibilities of output feedback design by applying a dynamic state observer. As a case study, we parameterize our model to Hungary, but it can be easily generalized to other countries as well.

2 Transmission dynamics model

2.1 Model description

We construct a compartmental model to describe the transmission dynamics of the infection, incorporating specific characteristics of COVID-19. Our population N is divided into the following classes, tracking the disease status of individuals: by S we denote the susceptibles, i.e. those who can be infected by the disease. Latent (L) are those who have already contracted the disease but do not show symptoms and are not infectious yet. Since transmission

may occur in the two days before the onset of symptoms [2], we consider a pre-symptomatic infectious compartment P. Since a large fraction of infected show only mild or no symptoms, after the incubation period, we differentiate infected individuals into asymptomatic (A) and symptomatic infected (I) compartments. Those in A will always recover, while the more severe cases in I may require hospitalization, in which case they move to compartment H, from where they may eventually recover (R) or die (D). We note that most transmission occurs within a few days after symptom onset, and the compartment I reflects this period of effective infectivity, rather than clinical status or PCR positivity, which may continue for weeks, yet we remove them from I and place them in R as they do not participate in chains of transmission anymore. Several studies [54,3,14,38,39,44] have proposed somewhat similar models for of COVID-19.

The compartmental model without any control terms reads as

$$S'(t) = -\beta \left[P(t) + I(t) + \delta A(t) \right] S(t)/N, \tag{1}$$
$$L'(t) = \beta \left[P(t) + I(t) + \delta A(t) \right] S(t)/N - \alpha L(t), \tag{2}$$
$$P'(t) = \alpha L(t) - pP(t), \tag{3}$$
$$I'(t) = qpP(t) - \rho_I I(t), \tag{4}$$
$$A'(t) = (1-q)pP(t) - \rho_A A(t), \tag{5}$$
$$H'(t) = \rho_I \eta I(t) - hH(t), \tag{6}$$
$$R'(t) = \rho_I(1-\eta)I(t) + \rho_A A(t) + (1-\mu)hH(t), \tag{7}$$
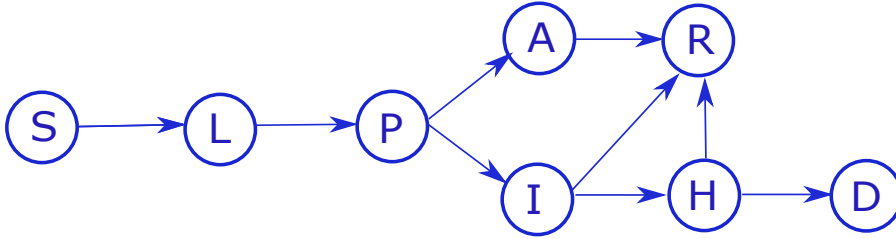$$D'(t) = \mu hH(t). \tag{8}$$

Fig. 1 Transition diagram. Circles represent compartments and arrows represent transitions between these compartments.

2.2 Model parameters

From the infectivity profile of COVID-19 [2], we can see that most transmissions occur between 3 days prior to and 4 days after symptom onset, with the pre-symptomatic infection fraction 43.7%. It is a good approximation to set the pre-symptomatic period p^{-1} as three days, and the symptomatic infectious

Parameter	Interpretation	Value	Reference
R_0	Basic reproduction number	2.2	[44]
α^{-1}	Latent period	2.5 (days)	[34]
p^{-1}	Pre-symptomatic infectious period	3 (days)	[2]
β	Transmission rate	1/3	calculated
δ	Relative transmissibility of asymptomatic	0.75	[9]
q	Prob. of developing symptoms	0.6	[9]
ρ_I^{-1}, ρ_A^{-1}	Infectious period	4 (days)	[2]
η	Hospitalization probability of symptomatic cases	0.076	[9]
h^{-1}	Average length of hospitalization	10 (days)	[15]
μ	Probability of fatal outcome, given hospitalization	0.145	[10]
N	Population size (Hungary)	9800000	[33]

Table 1 Parameters and values applied in the simulations

period ρ_I^{-1} as four days, with the same infectiousness β during this period. The estimated mean incubation period (which is the latent and pre-symptomatic period together) of the coronavirus disease is 5.5 days [34], thus the latent period α^{-1} is 2.5 days. Studies have shown similar durations of viral shedding between symptomatic and asymptomatic cases [58], so we set ρ_A^{-1} as four days as well. For the probability of developing symptoms, and the relative infectiousness of asymptomatic individuals, we use the CDC best estimate $q = 0.6$ and $\delta = 0.75$ [9]. The average stay in hospital is assumed to be 10 days, in accordance with the seven days median reported in [15]. The in-hospital death ratio (μ) in the USA is 0.145 [10]. The best estimate for the infection fatality rate (IFR) is 0.0065 [9], thus the hospitalization probability η of symptomatic cases can be inferred from the relation IFR $= q\eta\mu$ as $\eta \approx 0.076$.

The basic reproduction number, expressing the average number of new infections generated by a single infected individual in a fully susceptible population, is given as

$$R_0 = \beta \left(\frac{1}{p} + \frac{q}{\rho_I} + \frac{\delta(1-q)}{\rho_A} \right). \tag{9}$$

This formula can be derived as follows. Introduce a single infected individual into a susceptible population, then $S(t)/N \approx 1$. A newly infected individual, after passing through the latent phase, spends p^{-1} time in the pre-symptomatic compartment, while infecting others with rate β. Then transits to the symptomatic infected compartment with probability q, where it spends ρ_I^{-1} time infecting others again with rate β. Asymptomatic infection occurs with probability $1 - q$, in which case the individual infects with reduced rate $\delta\beta$, for time ρ_A^{-1} on average. Summing up these terms, we obtain (9). We assume that hospitalized individuals are properly isolated and do not cause significant numbers of infections.

Many studies have investigated R_0 for different countries, here we use $R_0 = 2.2$ estimated from the Hungarian data [44]. From relation (9), given that all other parameters are determined, we can calculate $\beta = 1/3$. We use Hungary's population size for N. The parameter values are summarized in Table 1.

3 The transmission dynamics model as a control system

To design a controller for the epidemic process, the first step is to define the manipulable parameters (control inputs) and identify the measured outputs. The latter comprises all relevant state dependent variables that are available for measurement. In the absence of vaccination, one needs to rely on a variety of non-pharmaceutical measures, which are aiming to prevent the transmission of the virus. In our model the control input, denoted by u, reflects the effect of the measures implemented to reduce the transmission rate. This variable is introduced in the model as a scaling factor of β, i.e. β is replaced by $\beta(1-u)$ in Eqs. (1) and (2) which are therefore modified to

$$S'(t) = -\beta(1 - u(t)) \left[P(t) + I(t) + \delta A(t)\right] S(t)/N, \tag{10}$$

$$L'(t) = \beta(1 - u(t)) \left[P(t) + I(t) + \delta A(t)\right] S(t)/N - \alpha L(t), \tag{11}$$

where $0 \le u(t) \le u_{max} < 1$, $\forall t \ge 0$. It is clear from the above equations that $u(t) = 0$ corresponds to unmitigated disease spread without any restriction, and $u(t) = u_{max}$ represents the strictest possible intervention level.

Analogously to R_0, the time dependent effective control reproduction number, denoted by $R_c(t)$, can be given by

$$R_c(t) = \beta\left(1 - u(t)\right) \frac{S(t)}{N} \left(\frac{1}{p} + \frac{q}{\rho_I} + \frac{\delta(1-q)}{\rho_A}\right). \tag{12}$$

An analysis of eleven European countries [21] revealed that the reproduction number (3.6 on average) dropped to 0.66 after the strictest lockdowns, hence we can assume $u_{max} = 0.82$.

3.1 Realization of the control input by specific control measures

Banned visits to health care institutions and long-term care facilities
Suspension of flights, international travel restrictions
University and school closures
Shortened opening time of shops
Stay at home measures
Restriction of gatherings, cancel public events
Suspend public transportation
Test, trace, isolate
Closing non-essential businesses
Emergency notification
Public information and awareness campaign
Mask wearing requirements

Table 2 Typical measures applied in various countries

Public health authorities are implementing a wide range of measures in response to the COVID-19 outbreak, see Table 3.1. There exist recent works

about the quantitative effect of different measures, usually in terms of the reduction of infection probabilities in different locations, e.g. in [57,50]. These can be used to match input value ranges and various possible restrictions. The Oxford COVID-19 Government Response Tracker [24] is a tool that systematically collects information on several different common policy responses on 17 indicators such as school closures and travel restrictions. Such indicators can be composed into indices, such as the government response stringency index. Having data from more than 160 countries, one can rigorously track the evolving policy responses around the world, and compare various countries. We have plotted the stringency index of selected European countries (that are similar to Hungary in population size) in Figure 2. Later we will see that the government responses of countries are very similar to constructed control inputs optimizing interventions with different cost functions and constraints.

Non-pharmaceutical measures aim to reduce the number of contacts between individuals, or reduce the probability of transmission when contact is made. The transmission rate can be considered as

$$\beta = \text{daily number of contacts} \times \text{transmission probability}.$$

Social distancing measures, such as school closures, banning of gatherings, and so on, reduce the average number of daily contacts made by an individual, while improved hygiene, mask wearing reduce the transmission probability. In our control system, we realize any combination of measures by changing β to $\beta(1-u)$, where the control input u represents the overall effect of measures in reducing transmission. For example, if the number of contacts are reduced to half by social distancing measures, then $\beta(1-u) = 0.5\beta$ thus $u = 0.5$ If both the contact number and the transmission probability are reduced to half by a combination of measures, then the transmission rate is reduced to its quarter, corresponding to $\beta(1-u) = 0.25\beta$, meaning that our control input is $u = 0.75$.

3.2 Discretization

The predictive control algorithm proposed in the next section requires a discrete-time dynamical model given in the general form $x_{k+1} = F(x_k, u_k)$. Therefore, the epidemic model (1) has to be discretized: function F has to be constructed s.t. $x_k \approx x(k \cdot T_s)$ for any piece-wise constant input $u(t) = u_k$, $t \in [k \cdot T_s, (k+1) \cdot T_s)$, where T_s is the sampling time and x_k is a state vector. From the different possible discretization methods we found that the simple forward Euler method is suitable for our purposes. It provides sufficient accuracy and preserves the structure of the continuous time model. We used a sampling time $T_s = 0.5$ days to get the discrete time model for control synthesis. It is important to note that the discrete time model is used for control input design, but the actual trajectories of the system between the sampling instants are computed by an appropriate ODE solver using a standard explicit Runge-Kutta (4,5) method. In Section 5 a dynamic observer is designed for
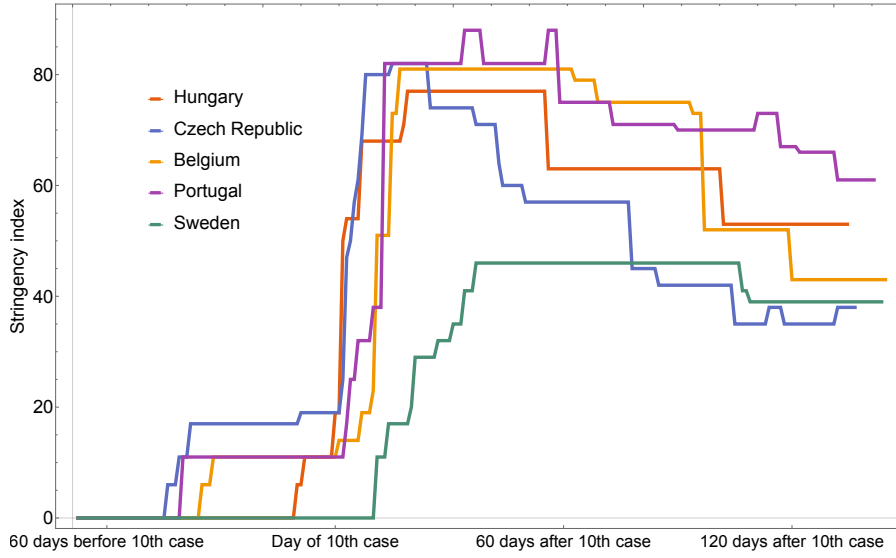
Fig. 2 Stringency index of control measures in some countries of similar population sizes (Hungary, Czech Republic, Sweden, Belgium, Portugal). The data is taken from [24], and shifted in time to match the day of 10th confirmed cases in each country.

the epidemic model, which also requires a discrete time model. To increase the accuracy, that model is generated by a smaller ($T_s = 0.1$ days) sampling time.

4 Constrained state feedback control for mitigation

4.1 Some relevant concepts from predictive control theory

In the first control scenarios the entire state vector is assumed to be known. This assumption is not realistic, but the corresponding simulation results will show the physical limitations for controlling the epidemic process in the ideal situation when full information is available. In Scenario 6, this assumption will be relaxed and only the number of hospitalized COVID-19 patients (state H in the model) and the number of deceased (state D in the model) will be considered available.

In all scenarios we design a feedback controller, i.e. the control input is periodically updated based on the actual measurements.

To formulate the control problem, the next step is to define the performance specifications that have to be satisfied by the controller and the controlled (closed loop) system. The most criteria we expect from a conscious epidemic management can naturally be formulated by cost functions to be minimized (e.g., healthcare costs, or the harmful effects of restrictions on economy and society) and constraints to be satisfied (e.g., upper bounds for the number of hospitalized people and/or on the number of deaths). Model Predictive

Control (MPC) methodology is therefore a promising approach for solving this problem. In the MPC framework the control synthesis is transformed into a constrained optimization task solved in every discrete time step, when the control input has to be updated. Since the synthesis procedure boils down to a standard optimization problem, theoretically a wide set of possible cost functions and complicated constraints can be handled.

Formally, in case of discrete-time models and full state measurement, the main steps of the MPC algorithm can be summarized as follows:

1. A suitable control horizon $M \in \mathbb{N}_+$ is chosen, the time counter k is set to 0.
2. At time $k \cdot T_s$, state x_k is measured. MPC is based on the prediction of the future states, therefore the following notation is introduced: the $(k+i)$th state predicted from the measurement made at time k will be denoted by $x_{k+i|k}$. By definition, $x_{k|k} = x_k$.
3. By applying the state update equation $x_{k+1} = F(x_k, u_k)$, the M predicted future states $\mathbf{x}_k = \{x_{k+1|k}, \ldots, x_{k+M|k}\}$ can be expressed as a function of the (yet unknown) future control actions $\mathbf{u}_k = \{u_{k|k}, \ldots, u_{k+M-1|k}\}$. Using this formulation an optimization problem can be defined:

$$\min_{\mathbf{u}_k} J(\mathbf{u}_k, \mathbf{x}_k) \tag{13a}$$

$$\text{w.r.t.} \quad x_{k+i+1|k} = F(x_{k+i|k}, u_{k+i|k}) \tag{13b}$$

$$G_x(\mathbf{x}_k) \leq h_x, \ G_u(\mathbf{u}_k) \leq h_u \tag{13c}$$

The objective function J and constraints (13c) are constructed to encode all design specifications to be satisfied by the controller and the closed loop system. To solve (13) an appropriate numerical solver has to be used. The result is the optimal input sequence $\mathbf{u}_k^* = \{u_{k|k}^*, \ldots, u_{k+N-1|k}^*\}$.

4. The first element of $\mathbf{u}_k^*$ is applied to the process, i.e. $u_k := u_{k|k}^*$. This control input is kept constant for T_s time period. Then k is incremented, i.e. $k := k + 1$, and the iteration continues at step 2.

We add the following important remarks to the MPC algorithm described above:

(a) In the description of the MPC above, we implicitly assumed that the system model is perfect: the model used for prediction is the same as that describes the true system behavior. In practical situations this rarely holds: there are modeling uncertainties that may corrupt the prediction and thus the control input obtained. It is known that an appropriate feedback can significantly reduce the effect of uncertainties in itself [47,29]. Moreover, there exist advanced methods for robust control synthesis and the robustness analysis of the closed loop. In this paper, no uncertainty is assumed for the model.

(b) The numerical complexity of the optimization problem depends on the structure of the cost functions and the constraints. Since the model is nonlinear, (13) becomes a nonlinear optimization problem. In the first control

scenarios we are going to investigate, quadratic cost function and linear constraints are used. Later, to formulate more complicated requirements, temporal logic constraints are also introduced, which turn the optimization task into a mixed integer nonlinear programming (MINLP) problem.

(c) The time horizon over which we intend to control the epidemic process is 180 days. We assume that the external conditions do not significantly change during this time period. Therefore, the behavior of the model beyond 180 days is not taken into consideration (if further control is needed, new computations must be performed after 180 days). Since the endpoint is fixed, the MPC is solved over shrinking horizon, i.e. M is time dependent and defined by $M_k = 180 - k$.

(d) If the entire state vector cannot be measured, the standard procedure is to augment the controller with a dynamical observer providing estimation for the true state. If the system is nonlinear, there is no general procedure for estimator design. This task can therefore be challenging: different existing methods have to be combined and adapted to the specific system model. In Section 5 we present a possible state estimator for the epidemic model above and show how it can be applied together with the MPC control.

(e) Although in the algorithm above the control input changes in every T_s time period, this is not necessary: the frequency of control update can be easily decreased by simple constraints on u.

4.2 Control scenarios

This section presents five control scenarios defined for the epidemic model. Each scenario addresses a different public health goal, and presents different control strategy. In all cases full state measurement is assumed and all simulations start from the same initial condition: $S_0 = N - L_0$, $L_0 = 40$, $P_0 = I_0 = A_0 = H_0 = D_0 = R_0 = 0$, where N is the population of Hungary according to Table 1. We assume that the epidemic remains undetected until the number of hospitalized patients exceeds a small threshold H_{thr}. Technically, this means that the simulation runs open loop until this threshold is reached, the controller is switched on only thereafter. In the case studies we examined, $H_{thr} = 10$ was used. As mentioned before, the sampling time is $T_s = 0.5$ days, but in each scenario the control input is updated only weekly, i.e. in every 14th time instant. The simulations were run on a Dell Vostro 5471 computer with i7-8550U (4 cores, 1.8-4.0 GHz) processor and 8GB RAM under MATLAB R2019b using the BARON 19.3.24 solver [30] and YALMIP version R20200116 [35]. The code for the translation of specifications containing temporal logic expressions to optimization problems was based on the BluSTL toolbox [16].

4.2.1 Scenario 1: Mitigation and suppression with continuous control input

In this scenario the control input is allowed to take arbitrary (continuous) values between 0 and an a-priori defined u_{max}. The cost function and constraints used in the MPC design are defined as follows:

$$J = \sum_{i=0}^{M} u_{k+i|k}^2 + w_H H_{M_k} + w_D D_{M_k} + w_\varepsilon \varepsilon, \qquad (14)$$

$$H_{k+i+1|k} \leq \overline{H} + \varepsilon, \quad 0 \leq \varepsilon, \quad 0 \leq u_{k+i|k} \leq u_{max}, \quad \forall i = 0 \ldots M - 1.$$

So, we would like to minimize the direct harmful effects of the restrictions (measured in a 2-norm), and keep the number of hospitalized patients under a predefined upper bound not to overload the healthcare system. The weighting factor w_D penalizing the number of deceased at the end of the horizon can be used to balance between *mitigation* and *suppression*, the two typical goals of COVID-19 management [20]. In the first case $w_D = w_H = 0$, so the focus is only on the direct cost of the control measures. The controller is expected to avoid strict measures and thus only mitigates the effects of the epidemic to the extent that the hospitalization remains below the given bound. In the second case $w_D \gg 0$, $w_H \gg 0$ are set such that the corresponding terms in the cost function are comparable with $\sum_{i=0}^{M} u_{k+i|k}^2$, so the controller tries to suppress the epidemic even if the control actions are expensive (i.e., they have harmful effects). The upper bound $\overline{H}$ represents the limit of the healthcare capacity. Parameters w_ε and ε are the ingredients of the soft constraint formulation. Soft constraint is applied to avoid the possible numerical infeasibility that can occur in the vicinity of $\overline{H}$ by the slight difference between the simulated continuous and the predicted discrete trajectories.

First the *mitigation* scenario is investigated. For this, simulations have been performed with the following parameter values: $\overline{H} = 10000$, $u_{max} = 0.82$. The results obtained are shown in Fig. 3. At the beginning of the control period the control input is small. This shows that less strict measures are sufficient during this time. As the epidemic progresses the control input slowly increases, but only until the 98th day, when it reaches a higher but still moderate value that is significantly smaller than the allowed maximum u_{max}. After the 98th day, the epidemic can be successfully mitigated. At the end of the control period (from day 154) the controller eases the restrictions (the control input decreases) since the control specifications have to be fulfilled only up to the 180th day, and this can be achieved even if the measures are relaxed (the control cost is decreased) in the last few weeks. If the constraints have to be satisfied on a longer time period, the control horizon has to be increased. From this result the following conclusion can be drawn: first, if we can intervene in time, there is no need to immediately implement strict measures, and second, the epidemic can be mitigated by applying only moderate restrictions. The total cost of the control strategy is $J_{1m}^* = 42.86$.

It is important to notice the increase of the state variables at the end of the horizon. Since finite time control policy is computed, it is not surprising
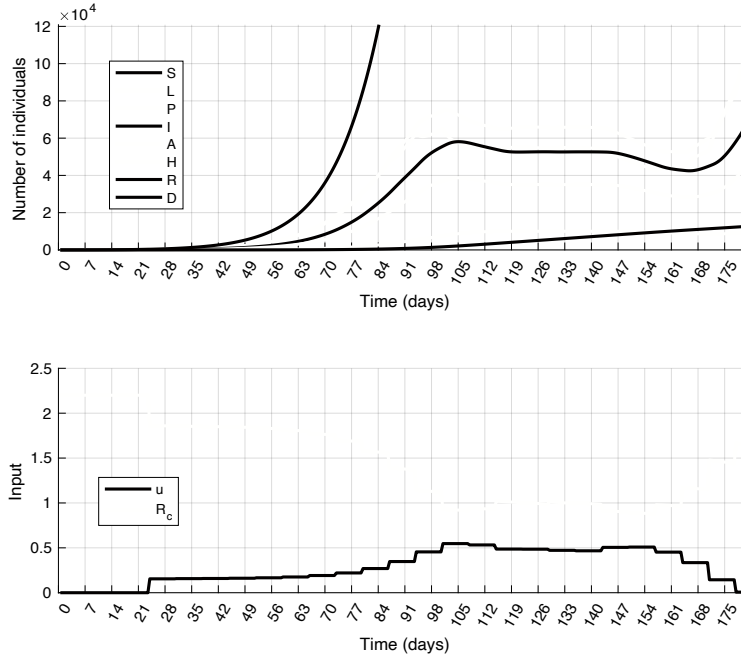
Fig. 3 Simulation results of Scenario 1.a (Mitigation): state trajectories (top) and control inputs with the corresponding effective reproduction number R_c (bottom).

that close to the end of the control period, the controller decreases the control input to minimize the cost. As a response, the state variables start to increase, but this does not cause feasibility problem as long as the constraints are not violated till the end of the horizon. This, so called "turnpike" behavior shows that easing the measures would result in an epidemic peak. With strict constraint on the healthcare capacity, this could be satisfactorily avoided only if a suitable herd immunity is reached by the end of the control horizon. It has been documented in several papers, e.g. [31] and [59] that in case of COVID-19 pandemic, to reach herd immunity without overwhelming the healthcare system would take years. Consequently, defining a good terminal constraint for this relatively small time period is not possible. What can be done is to directly constrain the increase of the states at the final (M and $M-1$-th) time instants [31]. We are going to show an example for this in Scenario 3.

Using the mitigation setup we have analyzed the maximal delay that the system can tolerate before implementing any measure. From a control perspective, this means that the system runs open loop (i.e., uncontrolled) in the time interval $[0, d \cdot T_s]$, where $d \in \mathbb{N}_+$ and then the controller is turned on. We seek the maximal d, for which the MPC optimization problem has a feasible solution. For the maximal tolerable delay we have obtained 74 days (i.e. $d = 144$). For larger values of d the MPC optimization has no feasible solution. (To detect infeasibility, a hard upper bound has been introduced for

the soft constraint violation. Specifically, in this scenario, $\varepsilon \leq 0.01$ has been used.) The simulation results are plotted in Figure 5. Considering the control input, it can be seen that as expected, the larger the delay the stricter the measures that have to be applied. The maximal control input is 0.82, which corresponds to total lockdown.

The controller for epidemic *suppression* has been designed by the following weights in the cost function: $w_D = 0.0267$ and $w_H = 0.0033$. The simulation results are plotted in Fig. 4. It is visible that the outbreak can be successfully suppressed for the price of a strict and early lockdown, followed by a slow gradual easing of the measures. However, a second wave of the epidemic appears at the end of the horizon as it has been observed in several countries, for example, the curves in Figure 4 show a striking resemblance to the true epidemic curve of Hungary . The total cost of the control strategy is $J_{1s}^* = 101.8$ from which the cost of the control input is $\sum_k u_k^2 = 89.27$.
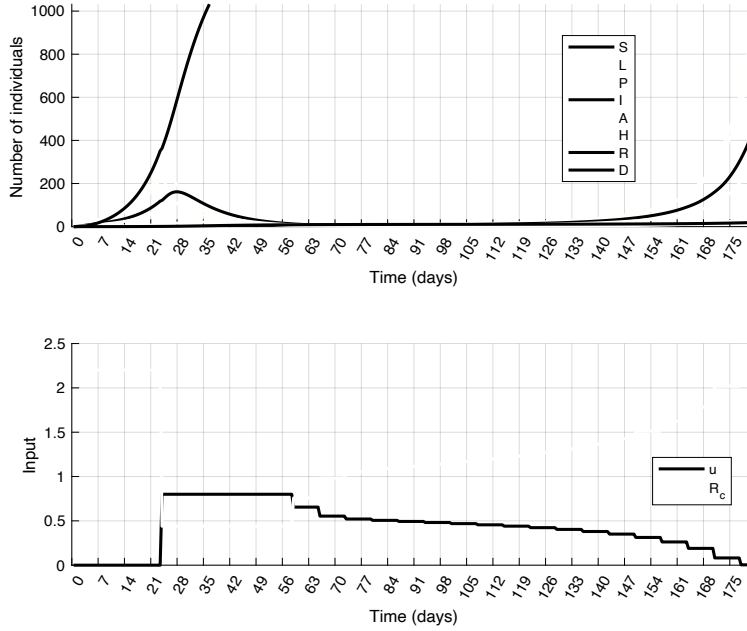

Fig. 4 Simulation results of Scenario 1.b (Suppression): state trajectories (top) and control inputs with the corresponding effective reproduction number R_c (bottom).

4.2.2 Scenario 2: The effect of control input quantization

By definition, the control input u reflects the effect of different measures implemented by the government in the society. Since there is a finite number of
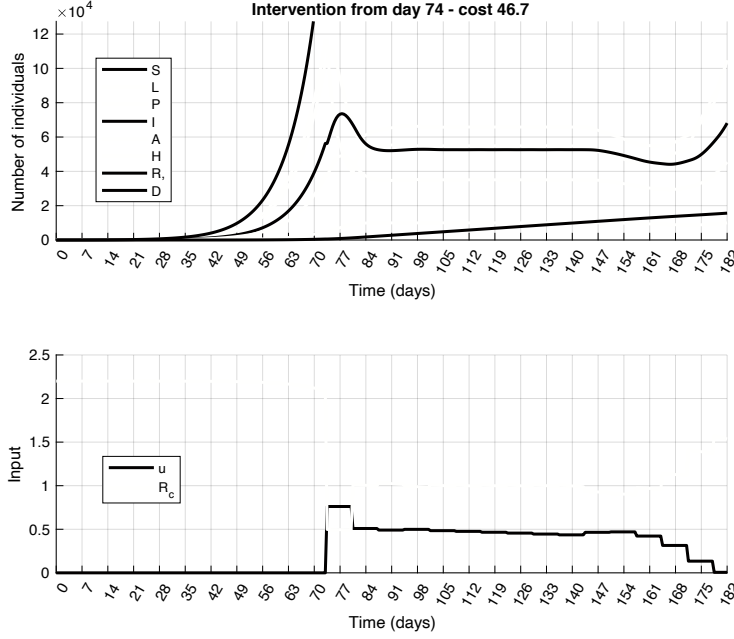
Fig. 5 Simulation results of Scenario 1.a with delayed intervention. Simulation results obtained at the maximal tolerable input delay ($d = 74$ days)

measures that can be applied (see Table 1), a control input with truly continuous range cannot be realized in practice. Motivated by this, we assume now that the control input is quantized and can take only 4 different values. Each value corresponds to a specific measure as follows: $u^{(1)} = 0, u^{(2)} = 0.19, u^{(3)} = 0.41, u^{(4)} = 0.6$. Here, as an example, $u^{(2)}$ may correspond to school closures, $u^{(3)}$ to stay-at-home orders, and $u^{(4)}$ can be interpreted as a combination of the two. To force $u_k \in \{u^{(1)}, u^{(2)}, u^{(3)}, u^{(4)}\}$ for all k, an additional constraint is added to the MPC synthesis:

$$\square(u = u^{(1)} \vee u = u^{(2)} \vee u = u^{(1)} \vee u = u^{(4)}), \qquad (15)$$

where $\square$ is a temporal logic operator called 'always' and is defined as follows: if ϕ is an arbitrary logical expression, then

$$\square_{[a,b]}\phi \text{ is true at time } t \Leftrightarrow \forall t' \in [t + a, t + b] \text{ the formula } \phi \text{ is true.} \quad (16)$$

Using this definition, constraint (15) prescribes that one of the four equations $u = u^{(i)}$, $i \in \{1, 2, 3, 4\}$ has always to be true. (More details on temporal logic operators can be found e.g. in [18]). We remark that the discrete inputs alone do not necessitate the application of temporal logic (see, e.g. [36]). However, this notation is intuitive, and using the temporal logic framework it is straightforward to add more complex (possibly time-varying) constraints as it will be shown by the next scenario.
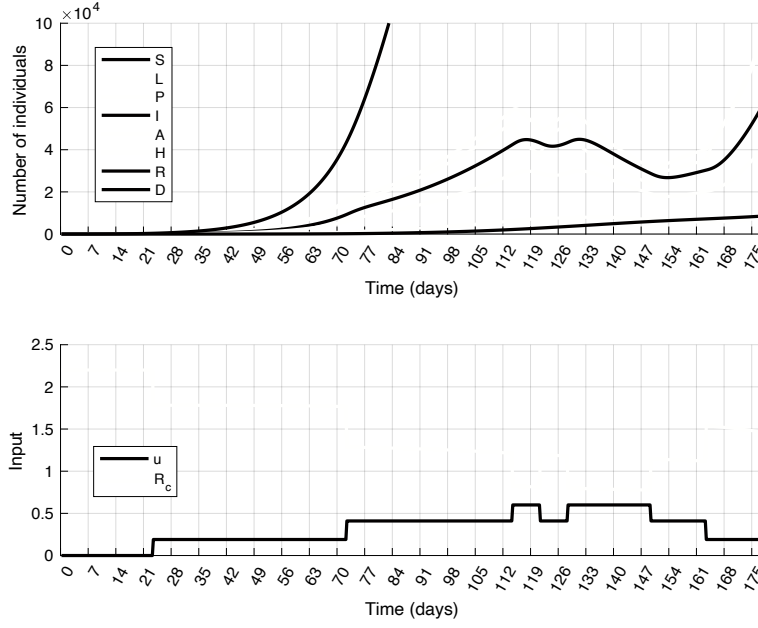
Fig. 6 Simulation results of Scenario 2 (Control input quantization): state trajectories (top) and control inputs with the corresponding effective reproduction number R_c (bottom).

To analyse the effect of input quantization we have performed the mitigation scenario defined in the previous section with the additional constraint (15). The results are plotted in Fig. 6. It can be seen that the primary control goal, i.e. the mitigation of the epidemic is achieved and the input and state constraints are satisfied. It is also important to mention that the quantized control input is similar to the continuous one obtained in Scenario 1, which means that the optimal control strategy is very similar in the two cases. On the other hand the quantization allows less freedom to the controller, so the total cost is now higher: $J_2^* = 45.88$.

4.2.3 Scenario 3: Refined constraint for healthcare capacity

In this scenario we allow, but only once and only for a limited time period, that the number of hospitalized patients (H) exceeds the limit $\overline{H}$. This scenario represents the case when there is an extra, but possibly costly reserve in the healthcare system that can be activated if necessary, or resources are reallocated to COVID-19 from other areas of healthcare. Formally, we introduce two new parameters: T_r and $\overline{\overline{H}}$, such that $\overline{H} < \overline{\overline{H}}$ and the MPC design is completed with the following constraint:

$$\Box(H \leq \overline{H}) \ \mathbf{U} \left(\Box_{[0, \ T_r]}(H \leq \overline{\overline{H}}) \wedge \Box_{[T_r, \ N]}(H \leq \overline{H}) \right) \tag{17}$$

where the temporal logic operator $\mathbf{U}$ (called 'until') is defined as follows:

$$\varphi \mathbf{U}_{[a,b]} \psi \text{ is true at time } t \Leftrightarrow \exists t' \in [t+a, t+b] \text{ st. } \psi \text{ is true } \wedge \tag{18}$$
$$\forall t'' \in [t, t'] \; \varphi \text{ is true} \tag{19}$$

In expression (17), $\overline{\overline{H}}$ denotes a new upper bound that is never to be violated and T_r is the maximal time period for which $H > \overline{H}$ is allowed. The numerical simulation for this scenario was performed with the following parameter values: $\overline{\overline{H}} = 15000$ and $T_r = 21$ days. The results obtained by performing a mitigation scenario are depicted in Fig. 7 and 8, respectively. Compared to the results of Scenario 1, it can be seen that the shapes of the control inputs are similar. The main difference is that the controller in Scneario 3 applies smaller control actions over almost the entire horizon. The control input is larger only for a short period after T_r is elapsed. This is necessary to stop the increase of the constrained state variables, which would result in the violation of the constraints and the loss of feasibility. Since the control input is smaller at most times than in Scenario 1, the total cost of the control is smaller: $J_{1m}^* = 42.86$ in Scenario 1 and $J_3^* = 41.43$ in Scenario 3.

Similar to the other scenarios investigated so far the state variables start to increase at the end of the control horizon. To avoid this behavior we introduce the following simple terminal constraint:

$$H_{k+M|k} + 1 \leq H_{k+M-1|k} \tag{20}$$

i.e. the number of hospitalized individuals must decrease in the last step. This constraint prevents H and the other states from increasing: strict control measures are applied till the very end of the horizon. Though the characteristic of the state variation has been significantly improved, nothing can be guaranteed for the process behavior beyond the control horizon. A later outbreak can be avoided only if the implementation of the carefully planned, strict control policy is continued.

5 State estimator design and output feedback control

In this section the assumption of full state measurement is dropped, and aligned with the common practice, only the number of the deceased (D) and the number of the hospitalized individuals (H) are monitored. There are examples in the COVID-19 literature, where the global dynamics and the epidemic curve was reconstructed from the data of hospitalized or deceased individuals [23,42] . In order to use the state feedback MPC controller, a dynamical observer is designed to estimate the remaining non-measured states.
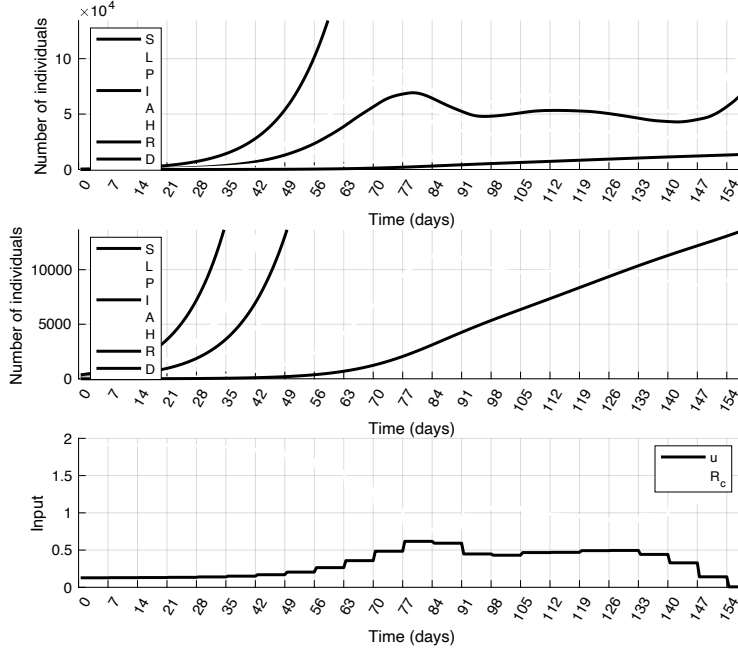
Fig. 7 Simulation results of Scenario 3 (Temporal increase of healthcare capacity): state trajectories (top) and control inputs (bottom) obtained with $T_r = 21$ and $\overline{\overline{H}} = 15000$. H is above 10000 between days 79 and 100.

5.1 LPV observer design for the epidemic model

To design the estimator, the states are normalized first and the dynamical model is divided into three parts. According to the three subsystems, the state vector is partitioned as follows: $s := S/N$, $\bar{x} = [L, P, I, A, H]/N$ and $r = R/N$. Focusing on x, we notice that the corresponding dynamical equations can be rewritten in linear parameter varying (LPV) form:

$$\bar{x}_{k+1} = (I + T_s A_0 + \rho_k T_s A_1)\bar{x}_k \doteq A(\rho_k)\bar{x}_k$$

where $\rho_k = s_k v_k$ with $v_k = 1 - u_k$ is the scheduling variable and

$$A_0 = \begin{bmatrix} -\alpha & 0 & 0 & 0 & 0 \\ \alpha & -p & 0 & 0 & 0 \\ 0 & qp & -\rho_I & 0 & 0 \\ 0 & (1-q)p & 0 & -\rho_A & 0 \\ 0 & 0 & \rho_I\eta & 0 & -h \end{bmatrix}, \quad A_1 = \begin{bmatrix} 0 & \beta & \beta & \delta\beta & 0 \\ 0 & 0 & 0 & 0 & 0 \\ 0 & 0 & 0 & 0 & 0 \\ 0 & 0 & 0 & 0 & 0 \\ 0 & 0 & 0 & 0 & 0 \end{bmatrix} \quad (21)$$

follow from (1). By introducing $C = [0\ 0\ 0\ 0\ 1]$, a measurement equation is added to the model: $y_H = C\bar{x}$, where $y_H = \bar{x}_5 = H/N$. Assume ρ is bounded, i.e. $\rho \in [\underline{\rho},\ \overline{\rho}]$ and $\underline{\rho}$, $\overline{\rho}$ are a-priori known. If we assume that up to half of
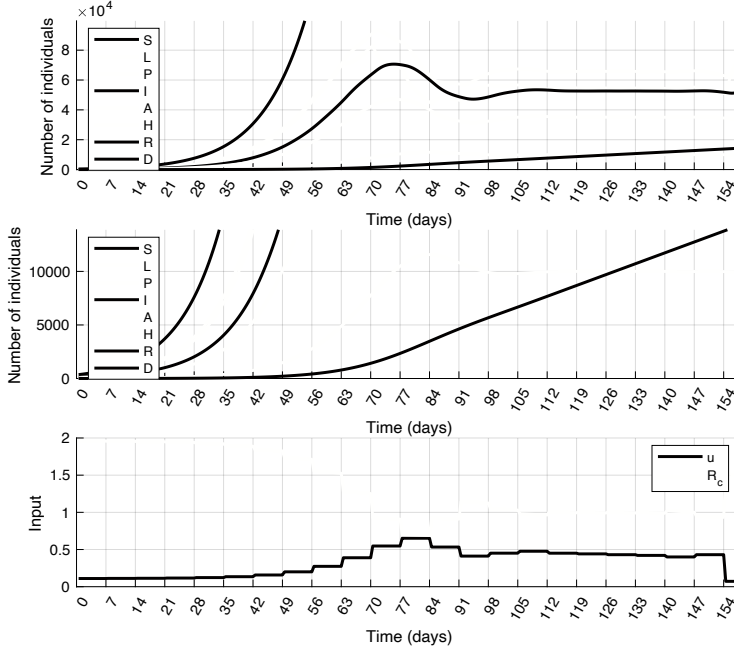
Fig. 8 Simulation results of Scenario 3 (Temporal increase of healthcare capacity): state trajectories (top) and control inputs (bottom) obtained with $T_r = 21$ and $\overline{\overline{H}} = 15000$. In this simulation a terminal constraint for the number of hospitalized individuals has also been introduced. H is above 10000 between days 76 and 97.

the population gets infected, then $s \in [0.5, 1]$ holds. This, together with the input constraint $u \in [0, 0.7]$ gives the bound for ρ: $\rho \in [0.15, 1]$. Using these bounds, a parameter varying observer can be designed, but in order to use it, the scheduling variable (ρ) has to be known at each time instant. Since in our case s_k is not available for measurement, we can only approximate it by using its difference equation, as follows:

$$\hat{s}_{k+1} = \hat{s}_k - T_s \hat{s}_k v_k \left[0 \ -\beta \ -\beta \ -\beta\delta \ 0 \right] \hat{\bar{x}} \tag{22}$$

By scheduling the model with $\hat{\rho} = \hat{s}v$ we face the problem of *observer design for LPV systems with inaccurately measured scheduling variables*. This problem is well identified in control literature and one possible solution is proposed in [37,11,25]. The papers discuss different variants, namely differently improved versions of the same approach introduced first in [37]. The method constructs a parameter varying observer, scheduled by $\hat{\rho}$ such that the boundedness of the estimation error is guaranteed as long as $\rho - \hat{\rho}$ is bounded.

Before applying this method, it is important to check the observability properties of the LPV model. The quickest analysis is to compute the observability matrix at different frozen (fixed) parameter values. This is a necessary

condition for the parameter dependent observability. Taking 10 equidistant points $\rho_1 \ldots \rho_{10}$ on the interval $[0.15, 1]$ we have found that the linear time-invariant (LTI) models $(A(\rho_i), C)$ are all observable: the corresponding observability matrices have full rank. However, it is important to note that these matrices are badly conditioned, they are close to singular, so the model is only weakly observable. This may challenge the observer design process and has effect on the achievable performance of the state estimation. It is also important to keep in mind that while the properties of the LPV model can give information on the properties of the nonlinear system, the two systems are not the same: the epidemic model is embedded in the LPV structure, so the latter describes a much broader dynamical behavior.

Starting from the LPV model, the state estimator is defined in the following form:

$$\hat{\bar{x}}_{k+1} = A(\hat{\rho})\hat{\bar{x}}_k + L(\hat{\rho})(y_H - \hat{y}_H) \tag{23}$$

where $\hat{y}_H = C\hat{x}$. This results in the following error dynamics:

$$e_{k+1} = \bar{x}_{k+1} - \hat{\bar{x}}_{k+1} = (A(\hat{\rho}) - L(\hat{\rho})C)e_k + \gamma_k \tag{24}$$

where $\gamma_k = (A(\rho_k) - A(\hat{\rho}_k))\bar{x}_k$. By fixing the feedback gain $L(\hat{\rho})$ in parameter affine form $L_0 + \hat{\rho}L_1$, the coefficient matrices L_0 and L_1 can be determined by finding positive definite P_i and general G_i, F_i matrices for $i \in \{1, 2\}$ that satisfy the following Linear Matrix Inequalities (LMI):

$$\begin{bmatrix} P_i & A_i^T G_i - C^T F_i^T \\ G_i A_i - F_i C & G_i^T + G_i - P_j \end{bmatrix} \succ 0, \ i, j \in \{1, 2\}, \tag{25}$$
$$A_1 = A(\underline{\rho}), \ A_2 = A(\overline{\rho}).$$

Then with $\bar{L}_i = G_i^{-1}F_i$, the observer gains are computed as follows: $L_1 = 1/(\overline{\rho} - \underline{\rho})(\bar{L}_2 - \bar{L}_1)$, $L_0 = \bar{L}_1 - \underline{\rho}L_1$. It is shown in [37], that the dynamics of the estimation error (24) is input-to-state stable (ISS) with respect to input γ_k. This implies that $e_k \to 0$ as $k \to \infty$ if $\gamma_k = 0$ (i.e. $\rho_k = \hat{\rho}_k$) and also that e_k is bounded for all k if $\rho_k - \hat{\rho}_k$ is bounded. Note that the observer design procedure considers the scheduling parameter independent of the state prediction. Formally this is true, as ρ_k depends on s_k which is not element of $\bar{x}_k$. Thinking in this way, the design is correct and the properties of the LPV observer can be independently analysed: for example, a bound for the ISS gain can be computed for (24) by using [37]. On the other hand, in our specific setup the dynamic equation (22) couples $\hat{\rho}$ and $\bar{x}$. This makes the analysis of the observer more challenging. We therefore make the further analysis via simulations by interconnecting the observer, the dynamics of $\hat{s}$ and the nonlinear system model.

In the possession of $\hat{s}$ and $\hat{x}$, the remaining state variable r can be obtained by iterating its state update equation:

$$\hat{z}_{k+1} = z_k + T_s[0 \ 0 \ \rho_I(1 - \eta) \ \rho_A \ (1 - \mu)h]\hat{\bar{x}}_k$$

Note, $\hat{r}$ is thus constructed by integrating the linear combination of the other states. We cannot prove anything for the boundedness of $z - \hat{z}$, but this is not a serious issue as r does not influence the behavior of the other states and it is used only in a control objective of Scenario 4. Since a lower limit for the number of infected patients is not a strict value, some deviation from the prescribed limit is not critical. Simulations will however reveal that $z - \hat{z}$ is actually small over the control horizon, so $\hat{z}_k$ is a suitably precise estimate for z_k. It is also important to mention that measurement D is not used in the observer. Since D does not influence the other state variables, measuring it is not relevant to the observer design (but it is very useful to precisely evaluate the cost function). It has to be admitted that the assumption of precisely knowing the model parameters is not completely realistic. Therefore, tracking the number of hospitalized people only may not be enough in practice to compute the population in other compartments with the required precision. To address this problem, the effect of parameter uncertainty for a controller-observer configuration is examined later in Subsection 5.4.

5.2 Numerical results obtained by the LPV observer

By solving (25), the following observer gains have been obtained:

$$
L_0 = \begin{bmatrix} 13.4913 \\ 14.1086. \\ 8.3603 \\ 5.5759 \\ 1.0058 \end{bmatrix}, \quad
L_1 = \begin{bmatrix} 1.3190 \\ 0.0767 \\ -0.0009 \\ -0.0019 \\ 0.0001 \end{bmatrix}. \tag{26}
$$

However, due to the weak observability, the error dynamics is close to the boundary of stability, the matrices P_1, P_2 characterizing the Lyapunov function are numerically ill-conditioned: there are several order of magnitude difference between their eigenvalues. Further analysis is thus necessary to reveal the performance properties of the observer, e.g. to compute an upper bound for the magnitude of the estimation error. Papers [11,25] refine the algorithm above and derive such a performance metric. In this paper we cannot go into the details of this analysis procedure, we examine the observer only in numerical simulations and place the focus on its application in closed loop control.

Figure 9 presents the simulation results obtained by running the system open-loop with the control input depicted in the same figure. The initial state was the same as we chosen above, i.e. $L_0 = 40$, $S = N - L$, and the other states are 0. In the simulation the normalized states were estimated, but they were re-scaled to plot the results. It can be seen that noticeable, but still not significant estimation error can be detected only in variables S and R and only in the neighborhood of the peak of the epidemic. This is not relevant however, since the estimator is intended to be used together with a controller, which mitigates or suppresses the epidemic peak.
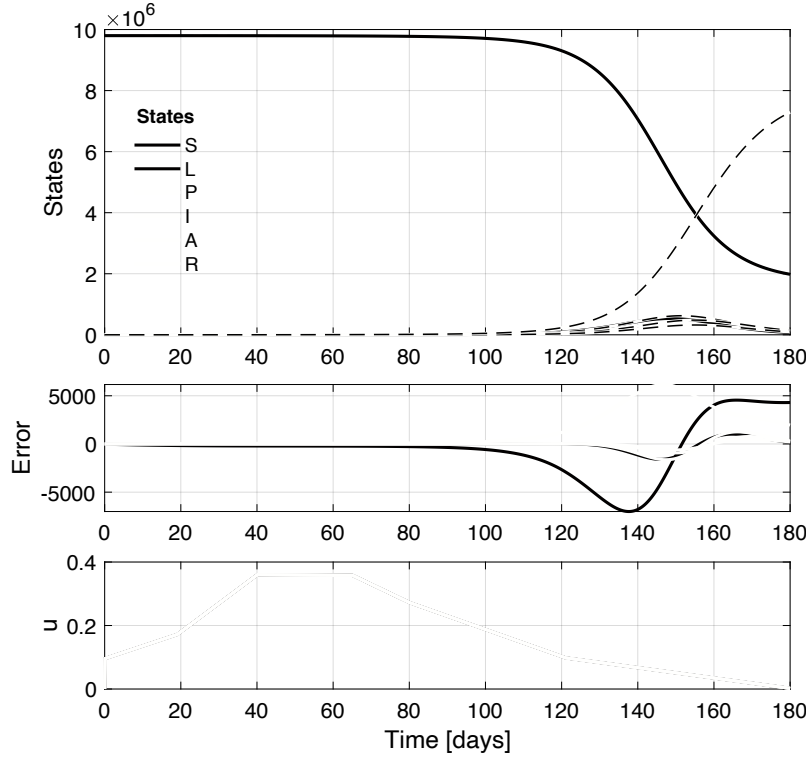
Fig. 9 True (coloured solid line) and estimated states (dashed black line) (top figure) and estimation error (middle figure) obtained by the state observer. The control input applied during the simulation is plotted in the bottom figure.

5.3 Scenario 4: Output feedback control

In this section we examine how the state observer works together with the MPC controller. For this, we repeat the simulation of Scenario 1 (subsection 4.2.1) with the following modification: the precise state measurement x_k is replaced by the estimated value $\hat{x}_k$. The simulation results are plotted in Figure 10. The control input and state trajectories obtained in the two scenarios can hardly be distinguished. Since the epidemic peak, where the estimation error would be noticeable, is mitigated, the state estimation is almost perfect over the entire horizon. Consequently, using $\hat{x}_k$ in the control input computation has only negligible effect on the closed-loop behavior. Compared to Scenario 1, the control costs are almost equal in the two scenarios: $J_1^* = 42.86$, $J_4^* = 42.98$. We can conclude that the lack of direct measurement of S is not crucial from the point of view of state measurement if the observer is used in closed-loop control.
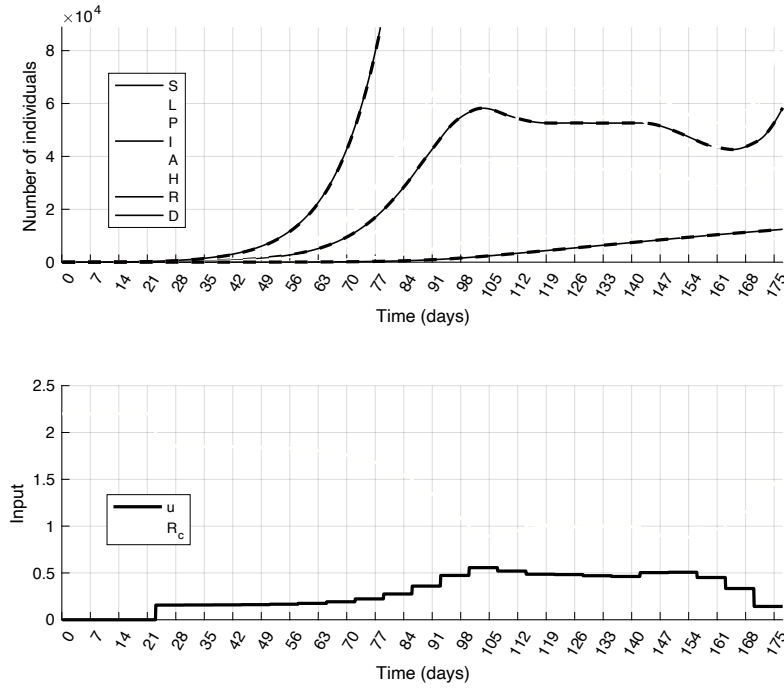
Fig. 10 Simulation results of Scenario 4 (Output feedback control): state trajectories (top) and control inputs with the corresponding effective reproduction number R_c (bottom). The true and estimated state trajectories are plotted by coloured solid and black dashed lines, respectively.

5.4 Scenario 5: Effect of parameter uncertainty

We have assumed so far that the dynamical model of the epidemic is precisely known, that is the model (1)-(8) with parameters in table 2.2 accurately describes the dynamical behavior of the epidemic process. This is hardly the case in a real situation. Therefore, the possible parameter uncertainties have to be taken into account during the control design process. This leads to a robust synthesis, which is beyond the scope of this paper. On the other hand, to study the applicability of the proposed control method, it is important to examine how it works in the presence of model mismatch. In this subsection we show several simulations with the output feedback scenario presented above with the following settings: the model structure used for prediction and state observation is the same, but certain parameters of the controlled system are different in each experiment. We assume that 4 parameters, namely α, q, δ, η are uncertain, they take values from the following intervals:

$$\alpha \in [1/3,\ 1/2],\ \delta \in [0.7,\ 0.8],\ q \in [0.5,\ 0.7],\ \eta \in [0.069,\ 0.083], \quad (27)$$

The upper and lower bounds of the parameter domains have been determined using the references in Table 1. Further, we assume that the other model pa-

Case number	α^{-1}	δ	q	η	cost	maxH
0	3.00	0.70	0.50	0.69	33.54	9305
1	3.00	0.70	0.50	0.83	35.33	9608
2	3.00	0.70	0.70	0.69	41.22	10290
3	3.00	0.70	0.70	0.83	43.79	10504
4	3.00	0.80	0.50	0.69	36.86	9738
5	3.00	0.80	0.50	0.83	38.96	9939
6	3.00	0.80	0.70	0.69	43.38	10781
7	3.00	0.80	0.70	0.83	46.30	10893
8	2.00	0.70	0.50	0.69	37.37	9336
9	2.00	0.70	0.50	0.83	39.65	9545
10	2.00	0.70	0.70	0.69	46.03	10242
11	2.00	0.70	0.70	0.83	49.20	10765
12	2.00	0.80	0.50	0.69	40.24	9691
13	2.00	0.80	0.50	0.83	44.64	9834
14	2.00	0.80	0.70	0.69	48.28	10651
15	2.00	0.80	0.70	0.83	51.70	11105

Table 3 Model parameters of the experiments performed for uncertainty analysis.

rameters are more precisely known, and therefore their nominal values were used in the simulations. We remark that possible uncertainty in β can be handled, since due to the model structure, designing for larger β gives a feasible controller for smaller values as well. To analyze the robustness, 16 simulations defined by the possible combinations of the min-max values of the uncertain parameters have been performed. Table 5.4 collects the parameters of the experiments with the results obtained. The detailed simulation results obtained for cases 7 and 15 are plotted in Figs. 11 and 12, respectively.

It can be seen that the controller worked acceptably well with uncertain models, although the cost varied visibly for the different cases. Regarding the constraint on the health care capacity, it is only violated in half of the simulations and the transgression of the limit is not critical. On the other hand, there is a room for performance improvement, and thus improving the robustness of the controller is an important task in the future.

6 Discussion

The model-based control of the spread of the COVID-19 epidemic was proposed in this paper. The dynamical model is given in the form of a set of nonlinear ODEs containnig 8 compartments. The model parameters were determined from the literature and the epidemic data recorded in Hungary between March and May, 2020. The assumed manipulable control input with strict upper and lower bounds is the time-varying transmission rate affected by different restrictive measures planned and implemented by the authorities to slow down disease spread.

A model-predictive control approach was proposed which uses the discrete-time version of the dynamical model and is able to take into consideration complex specifications and constraints containing even integer variables and
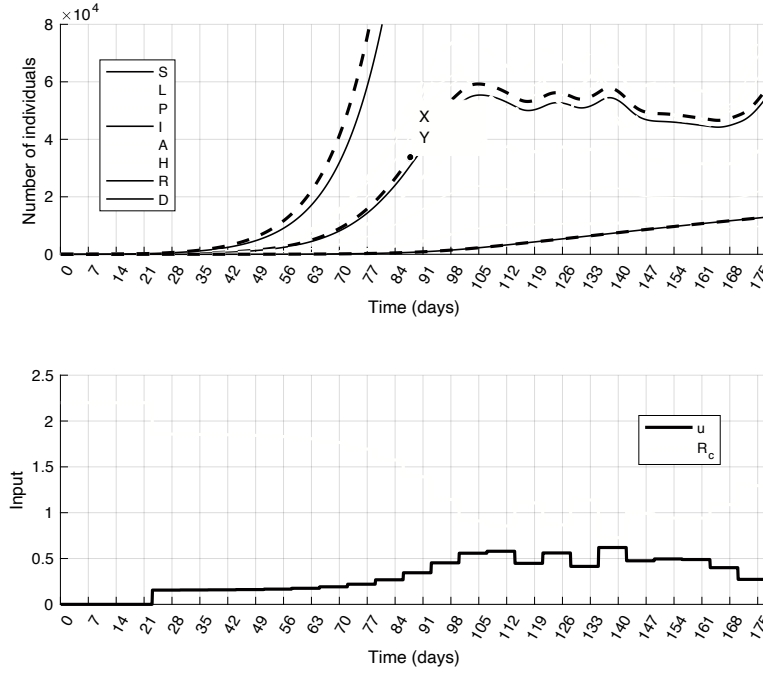
Fig. 11 Simulation results of Scenario 5 (Output feedback control) with model uncertainties. State trajectories (top) and control inputs with the corresponding effective reproduction number R_c (bottom) in case 7 of table 5.4. The true and estimated state trajectories are plotted by coloured solid and black dashed lines, respectively.

logical relations in the form of temporal logic expressions. The control goals are then automatically translated to a MINLP problem, capable of handling the nonlinear system dynamics. To address the realistic situation when not all state variables are observed continuously, a state observer is proposed using the theory of LPV systems, assuming that only the number of hospitalized and deceased patients are known on a daily basis. In the numerical simulations we found that the number of people in the other 6 compartments can be computed with sufficient precision using the observer if the model parameters are known, although the model itself is numerically only weakly observable due to the possible different orders of magnitudes of the susceptible and the infected population. This underlines the importance of regularly tracking the susceptible population (which is a scheduling parameter in the state observer), since the on-line estimation of the other states could be significantly improved by that. In practice, this can be achieved by large scale serological surveys.

Five control scenarios were shown and analyzed with different goals and assumptions. The scenarios cover the well-known cases of mitigation, when the direct cost of the intervention (control) is minimized with a constraint on healthcare capacity, and also suppression, where the cost is assigned to
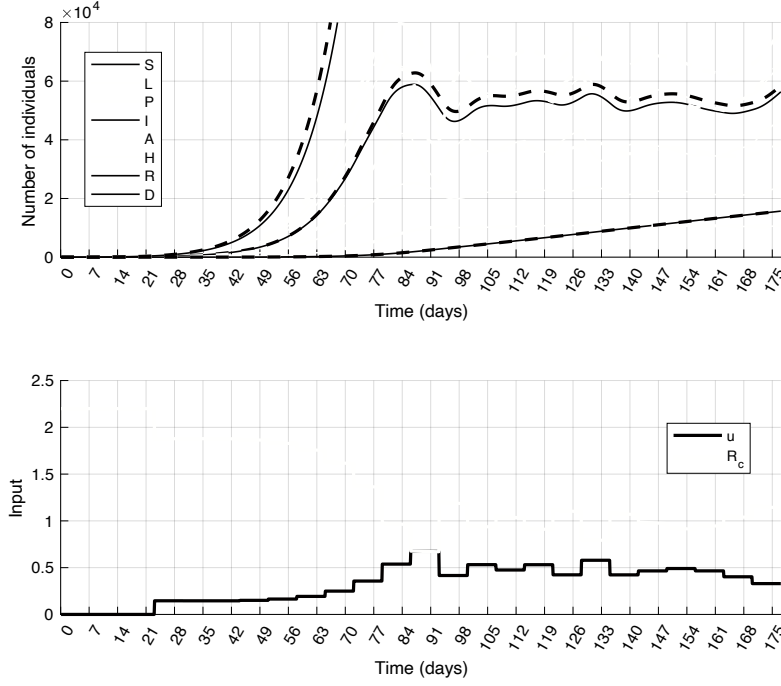
Fig. 12 Simulation results of Scenario 5 (Output feedback control) with model uncertainties. State trajectories (top) and control inputs with the corresponding effective reproduction number R_c (bottom) in case 15 of table 5.4. The true and estimated state trajectories are plotted by coloured solid and black dashed lines, respectively.

infection, hospitalization and fatalities. It is worthwhile to note that there is a striking resemblance between the constructed control inputs and real life government responses, measured by a stringency index, both for mitigation and suppression strategies. We have also monitored the time varying effective reproduction number R_t, which became a very popular measure of the current epidemic situation during the COVID-19 pandemic. For suppression, we see that very strict measures (lockdown) are necessary initially, and they can be slowly relaxed later. This corresponds to a sharp drop in R_t to levels way below one. On the other hand, for mitigation, the stringency of the control is increased much more slowly, and maximized at a moderate level, while R_t is being kept around the critical value 1 for a long time period.

We emphasize that the proposed flexible approach is able to directly handle predefined discrete levels of restrictions. The output feedback design case (i.e., the combination of the controller and observer) was also examined through several simulations assuming uncertainties in selected parameters. It is justified by the computational results that an early intervention is of key importance in satisfying the control goals and constraints. The feasibility analysis corresponding to the model predictive control problem is also useful to assess the

practical (physical, biological) limits of the planned interventions and identify late actions. Future work will be focused on the sensitivity and further robustness analysis of the approach and on the specification of even more realistic goals and constraints. Among the latter, assigning individual costs to different types of restrictions (see Table 2) and putting the optimal selection between them into the framework of optimal control may add further value to the research.

Acknowledgement

Conflict of Interest:

The authors declare that they have no conflict of interest.

References

1. Ames, A. D., Molnar, T. G., Singletary, A. W., Orosz, G. (2020). Safety-Critical Control of Active Interventions for COVID-19 Mitigation. medRxiv, doi: https://doi.org/10.1101/2020.06.17.2013326
2. Ashcroft, P., Huisman, J. S., Lehtinen, S., Bouman, J. A., Althaus, C. L., Regoes, R. R., & Bonhoeffer, S. (2020). COVID-19 infectivity profile correction. arXiv preprint arXiv:2007.06602.
3. Barbarossa, M.V. *et al.* A first study on the impact of current and future control measures on the spread of COVID-19 in Germany. *medRχiv* **2020.04.11.** https://doi.org/10.1101/2020.04.08.20056630.
4. Becker, N.G.: Modeling to inform infectious disease control, vol. 74. CRC Press (2015)
5. Belta, C., Yordanov, B., Gol, E.A.: Formal methods for discrete-time dynamical systems, vol. 89. Springer (2017)
6. Boldog P.; Tekeli, T.; Vizi, Zs.; Dénes, A.; Bartha, F.A.; Röst, G. Risk Assessment of Novel Coronavirus COVID–19 Outbreaks Outside China. *J. Clin. Med.* **2020**, *9(2)*, 571. https://doi.org/10.3390/jcm9020571.
7. Böhmer, M.M. *et al.* Investigation of a COVID-19 outbreak in Germany resulting from a single travel-associated primary case: a case series. *The Lancet Infectious Diseases* **2020.05.15.** https://doi.org/10.1016/S1473-3099(20)30314-5.

8. Bussell, E.H., Dangerfield, C.E., Gilligan, C.A., Cunniffe, N.J.: Applying optimal control theory to complex epidemiological models to inform real-world disease management. Phylosophical Transactions B of the Royal Society **374**, 20180284 (2018). DOI 10.6084/ m9.figshare.c.4462796

9. CDC COVID-19 Pandemic Planning Scenarios, US CDC, `https://www.cdc.gov/ coronavirus/2019-ncov/hcp/planning-scenarios.html`

10. COVID-NET, A weekly summary of U.S. COVID-19 Hospitalization Data, `https:// gis.cdc.gov/grasp/COVIDNet/COVID19_5.html`

11. Daafouz, J., Millerioux, G., Rosier, L.: Observer design with guaranteed bound for LPV systems. IFAC World Congress, 107–112 (2005)

12. de la Sen, M., Alonso-Quesada, S.: Vaccination strategies based on feedback control techniques for a general SEIR-epidemic model. Applied Mathematics and Computation **218**, 2888–3904 (2011)

13. Deslandes, A. SARS-CoV-2 was already spreading in France in late December 2019. *Int. J. Antimicrob. Agents* **2020**, 106006. `https://doi.org/10.1016/j.ijantimicag.2020. 106006`.

14. Di Domenico, L. *et al.* Expected impact of lockdown in Île-de-France and possible exit strategies. *medRχiv* **2020.04.17.** `https://doi.org/10.1101/2020.04.13.20063933`

15. Docherty, A.B. *et al.* Features of 16,749 hospitalised UK patients with COVID-19 using the ISARIC WHO Clinical Characterisation Protocol. *medRχiv* **2020.04.28.** `https: //doi.org/10.1101/2020.04.23.20076042`.

16. Donzé, A., Raman, V.: BluSTL: Controller synthesis from signal temporal logic specifications. 1st and 2nd International Workshop on Applied Verification for Continuous and Hybrid Systems, EPiC Series in Computer Science **34**, 160–168 (2015)

17. ECDC. Rapid Risk Assessment: Resurgence of reported cases of COVID 19 in the EU/EEA, the UK and EU candidate and potential candidate countries *Europen Centre for Disease Prevention and Control* **2020.07.02.** `https://www.ecdc.europa.eu/sites/default/files/documents/ RRA-Resurgence-of-reported-cases-of-COVID-19-in-the-EU-EEA.pdf`.

18. Farahani, S.S., Raman, V., Murray, R.M.: Robust model predictive control for signal temporal logic synthesis. IFAC-PapersOnLine **48**(27), 323–328 (2015)

19. Feng, Z., 2014. Applications of epidemiological models to public health policymaking: the role of heterogeneity in model predictions. World Scientific.

20. Ferguson N.M. *et al.* Report 9 – Impact of non-pharmaceutical interventions (NPIs) to reduce COVID-19 mortality and healthcare demand. *Imperial College London* **2020.03.16.** `https://www. imperial.ac.uk/mrc-global-infectious-disease-analysis/covid-19/ report-9-impact-of-npis-on-covid-19`.

21. Flaxman, S., Mishra, S., Gandy, A., et al. (2020). Estimating the effects of non-pharmaceutical interventions on COVID-19 in Europe. Nature, 1-5.

22. Giordano, G., Blanchini, F., Bruno, R., Colaneri, P., Di Filippo, A., Di Matteo, A., Colaneri, M.: Modelling the covid-19 epidemic and implementation of population-wide interventions in italy. Nature Medicine pp. 1–6 (2020)

23. Golding, N., Russell, T.W., Abbott, S., Hellewell, J., Pearson, C.A., van Zandvoort, K., Jarvis, C.I., Gibbs, H., Liu, Y., Eggo, R.M. and Edmunds, J.W.: . Reconstructing the global dynamics of under-ascertained COVID-19 cases and infections. medRxiv 2020.07.07.20148460; doi: `https://doi.org/10.1101/2020.07.07.20148460` (2020)

24. Hale, T., Angrist N, Petherick, A., Phillips, T. & Webster, S. (2020). Variation in government responses to COVID-19. Blavatnik School of Government Working paper, BSG-WP-2020/032 `https://www.bsg.ox.ac.uk/research/research-projects/ coronavirus-government-response-tracker`

25. Heemels, W. P. M. H., Daafouz, J., Millerioux, G.: Observer-Based Control of Discrete-Time LPV Systems With Uncertain Parameters. IEEE Transactions on Automatic Control **55**(9), 2130–2135 (2010).

26. Hernandez-Vargas, E.A.: Modeling and Control of Infectious Diseases in the Host: With MATLAB and R. Academic Press (2019)

27. Ibeas, A., de la Sen, M., Alonso-Quesada, S., Zamani, I., Shafiee, M.: Observer design for seir discrete-time epidemic models. In: 2014 13th International Conference on Control Automation Robotics & Vision (ICARCV), pp. 1321–1326. IEEE (2014)

28. Iggidr, A., Souza, M.O.: State estimators for some epidemiological systems. Journal of Mathematical Biology **78**(1-2), 225–256 (2019)
29. Isidori, A.: Nonlinear Control Systems. Springer, Berlin (1999)
30. Khajavirad, A., Sahinidis, N.V.: A hybrid LP/NLP paradigm for global optimization relaxations. Mathematical Programming Computation **10**, 383–421 (2018)
31. Köhler, J., Schwenkel, L., Koch, A., Berberich, J., Pauli, P., Allgöwer, F.: Robust and optimal predictive control of the covid-19 outbreak. arXiv preprint arXiv:2005.03580 (2020)
32. Kronqvist, J., Bernal, D.E., Lundell, A., Grossmann, I.E.: A review and comparison of solvers for convex MINLP. Optimization and Engineering **20**(2), 397–455 (2019)
33. KSH, Hungarian Central Statistical Office, `http://www.ksh.hu/?lang=en`
34. Lauer, S. A., Grantz, K. H., Bi, Q., Jones, F. K., Zheng, Q., Meredith, H. R., ... & Lessler, J. (2020). The incubation period of coronavirus disease 2019 (COVID-19) from publicly reported confirmed cases: estimation and application. Annals of internal medicine, 172(9), 577-582.
35. Löfberg, J.: YALMIP : A Toolbox for Modeling and Optimization in MATLAB. In Proceedings of the CACSD Conference, (2004)
36. Morato, M. M., Bastos, S. B., Cajueiro, D. O., & Normey-Rico, J. E. (2020). An Optimal predictive control strategy for COVID-19 (SARS-CoV-2) social distancing policies in Brazil. arXiv preprint arXiv:2005.10797 [q-bio.PE]
37. Millerioux, G., Rosier, L., Bloch, G., Daafouz, J.: Bounded state reconstruction error for LPV systems with estimated parameters. IEEE Transactions on Automatic Control **49**(8), 1385–1389 (2004).
38. Moghadas, S.M. *et al.* Projecting hospital utilization during the COVID-19 outbreaks in the United States. *Proc. Natl. Acad. Sci. U.S.A.* **2020**, *117(16)*, 9122–9126. `https://doi.org/10.1073/pnas.2004064117`.
39. Moss, R. *et al.* Modelling the impact of COVID-19 in Australia to inform transmission reducing measures and health system preparedness. *medRχiv* **2020.04.11.** `https://doi.org/10.1101/2020.04.07.20056184`.
40. Muqbel K., Vas G., Röst G.: Periodic orbits and global stability for a discontinuous SIR model with delayed control Qualitative Theory of Dynamical Systems 19, 59 (2020)
41. Nowzari, C., Preciado, V.M., Pappas, G.J.: Analysis and control of epidemics: A survey of spreading processes on complex networks. IEEE Control Systems Magazine **36**(1), 26–46 (2016)
42. Pugliese, A., Sottile, S.: Inferring the COVID-19 infection curve in Italy. arXiv preprint arXiv:2004.09404 (2020).
43. Riobello, R.N.: On some new mathematical models of infectious diseases: analysis, equilibrium, positivity and vaccination controls. Ph.D. thesis, University of Basque Country, Spain (2015)
44. Röst G, Bartha F, Bogya N, Boldog P, Dénes A, Ferenci T, Horváth JK, Juhász A, Nagy Cs, Tekeli T, Vizi Zs, Oroszi B, Early phase of the COVID-19 outbreak in Hungary and post-lockdown scenarios, Viruses 2020, 12(7), 708; `https://doi.org/10.3390/v12070708`
45. Sebastiani, G.; Massa, M.; Riboli, E. Covid–19 epidemic in Italy: evolution, projections and impact of government measures. *Eur. J. Epidemiol.* **2020**, *35*, 341–345. `https://doi.org/10.1007/s10654-020-00631-6`.
46. Sélley, F., Besenyei, A., Kiss, I.Z., Simon, P.L.: Dynamic control of modern, network-based epidemic models. SIAM Journal on Applied Dynamical Systems **14**(1), 168–187 (2015)
47. Sontag, E.D.: Mathematical Control Theory: Deterministic and Finite Dimensional Systems. Springer (1998)
48. Stewart, G., Heusden, K. and Dumont, G.A., 2020. How control theory can help us control COVID-19. IEEE Spectrum, 57(6), pp.22-29.
49. Stoecklin, S.B. *et al.* First Cases of Coronavirus Disease 2019 (COVID-19) in France: Surveillance, Investigations and Control Measures, January 2020. *Euro Surveill.* **2020**, *25(6)*. `https://doi.org/10.2807/1560-7917.es.2020.25.6.2000094`.
50. Ullah, S., Khan, M.: Modeling the impact of non-pharmaceutical interventions on the dynamics of novel coronavirus with optimal control analysis with a case study. Chaos, Solitons and Fractals **139** (2020). DOI 10.1016/j.chaos.2020.110075.

51. Wang, H., Wang, Z., Dong, Y., et al.: Phase-adjusted estimation of the number of coronavirus disease 2019 cases in Wuhan, China. Cell Discovery **6** (2020). DOI 10.1038/s41421-020-0148-0. Article number 10

52. Wang, Z., Röst, G., Moghadas, S.M.: Delay in booster schedule as a control parameter in vaccination dynamics Journal of Mathematical Biology, 79:(5-6), pp 2157–2182 (2019)

53. Watkins, N.J., Nowzari, C., Pappas, G.J.: Robust economic model predictive control of continuous-time epidemic processes. IEEE Transactions on Automatic Control **65**(3), 1116–1131 (2020). DOI 10.1109/TAC.2019.2919136.

54. Weitz, J.S. COVID-19 Epidemic Risk Assessment for Georgia. *Github* **2020.03.24.** `https://github.com/jsweitz/covid-19-ga-summer-2020`.

55. Wiersinga WJ, Rhodes A, Cheng AC, Peacock SJ, Prescott HC. Pathophysiology, Transmission, Diagnosis, and Treatment of Coronavirus Disease 2019 (COVID-19): A Review. JAMA. Published online July 10, 2020. `doi:10.1001/jama.2020.12839`

56. WHO Situation report - 191, Coronavirus disease 2019 (COVID-19) 29 July 2020 `https://www.who.int/docs/default-source/coronaviruse/situation-reports/20200729-covid-19-sitrep-191.pdf`

57. Wu, J., Tang, B., Bragazzi, N., Nah, K., McCarthy, Z.: Quantifying the role of social distancing, personal protection and case detection in mitigating COVID-19 outbreak in Ontario, Canada. Journal of Mathematics in Industry **10**(1) (2020).

58. Zou L, Ruan F, Huang M, et al. SARS-CoV-2 Viral Load in Upper Respiratory Specimens of Infected Patients. N Engl J Med. 2020;382(12):1177-1179

59. Helmholtz-Initiative 'Systemische Epidemiologische Analyse der Covid-19-Epidemie', Stellungnahme der Helmholtz-Initiative 'Systemische Epidemiologische Analyse der COVID-19-Epidemie', 2020.